Proceedings of the Thirty-second (2022) International Ocean and Polar Engineering Conference **www.isope.org**
Shanghai, China, June 5–10, 2022

ISBN 978-1-880653-81-4; ISSN 1098-6189

Analysis of wave-induced abrasion on a slit-type seawall along a rocky coastline

Shota Abe
Yachiyo Engineering Co., Ltd
Taito, Tokyo Japan
Katsutoshi Kimura
Department of Architecture and Infrastructure, Muroran Institute of Technology
Muroran, Hokkaido, Japan
Takao Nakoshi
Hokkaido Road Management Engineering Center
Sapporo, Hokkaido Japan
Yasuji Yamamoto
Department of Civil and Environment Engineering, Hokkaido University of Science
Sapporo, Hokkaido Japan
Yoshihiro Murata
Civil Engineering Consultant Sapporo Branch
Sapporo, Hokkaido Japan

ABSTRACT

The research reported here involved clarification of the process of wave-related abrasion on a slit-type seawall along a rocky coastline, with investigation of the movement characteristics of 100 kg of stones via hydraulic experiments with a model scale of 1/20. Abrasion damage was generally observed near the still water level with correspondence to the position with the highest collision ratio, which was higher for longer wave periods. The relationship between wave height and collision speed was clarified from analysis of video on stone movement patterns relating to wave action. The characteristics of flow patterns and overtopping waves were investigated up to design wave conditions via hydraulic experiments with a model scale of 1/40, and seawall abrasion was estimated as 10 mm/year (similar to the observation value) using an experimental formula based on local wave data. Damage repair was also proposed from the wave overtopping test results, with concrete filling of worn parts and placement of wave-dissipating blocks found to be an optimal approach.

KEY WORDS: rocky coast; slit-type seawall; abrasion; stones; repair; field observation; hydraulic experiment

INTRODUCTION

Deformation of concrete structures along rocky coastlines due to stone motion caused by wave action often progresses rapidly, seriously affecting seawall safety and the anti-wave performance of related background facilities. To elucidate the status of such abrasion, Watanabe, et al.(2013) researched concrete-block erosion along the Shimoniikawa coast of Japan's Toyama Prefecture and the Suruga and Numazu coasts of Shizuoka Prefecture, reporting larger abrasion volumes around an elevation of still water level (T.P. 0.0 m). Abrasion research conducted by Matsuda et al. (2007) regarding coastal bridge piers on the Hokuriku Expressway in Ishikawa Prefecture also revealed an abrasion rate of approximately 10 mm/year. Oide et al. (2018) further reported a risk of tunnel collapse along the Ogon route in the Hiroo area of Hokkaido due to ongoing abrasion to the lower levels of block masonry.
The study reported here was conducted to investigate abrasion of a slit-type seawall (Fig. 1) along a rocky Sea of Japan coastline in Hokkaido, and elucidated the movement characteristics of stones based on hydraulic model experiments. The seawall abrasion rate was estimated using data collected at the local NOWPHAS station using an experimental formula, and a wave overtopping test was conducted to establish a repair technique for such damage.

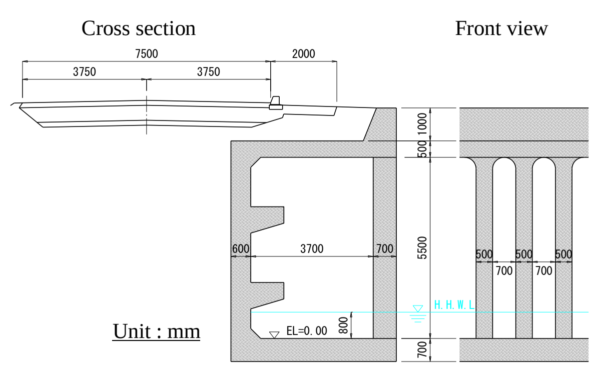

Fig. 1 Slit-type seawall

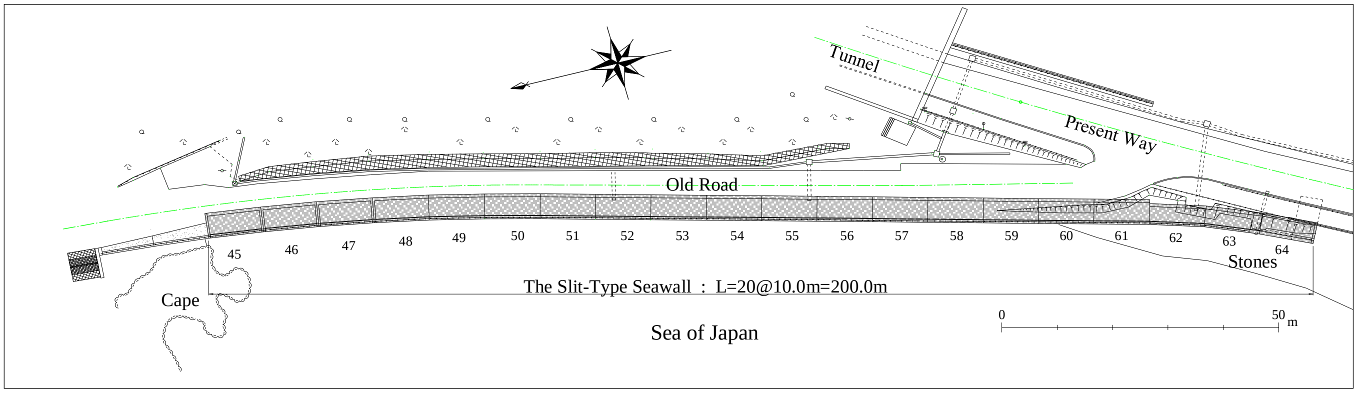

Fig. 2 Target coastal area

ON SITE ABRASION

Coastal landform characteristics

The 200-m seawall was constructed between 1988 and 1990 for a west-north-west road along the Sea of Japan. The surrounding sea is calm in summer but otherwise subject to waves caused by north-westerly seasonal winds. The water was deepest near the reef of the cape and shallower toward the right (Fig. 2). The shoreline was situated near slit no. 60, and stones with diameters of 10 to 30 cm had accumulated on the land side. The seawall faced an old road with a two-lane road immediately above.

Seawall abrasion research

Photo 1, showing the inside of the seawall from abrasion field surveys conducted in 2004 and 2017, indicates stone accumulation in the water-retarding chamber. Photo 2 shows abrasion progress on pillars and bottom plates, with exposed reinforcements in some parts. Abrasion depth was measured on the front, sides and back of pillars and between those on the bottom plate.

Relationship between abrasion volume and water depth

Figure 3 shows the planar distribution of abrasion depth at pillar fronts in 2004 and 2017 as well as ground height above/below T. P. in front of the pillar. Abrasion occurred in a 70-m section between slits 58 and 64, where the water was shallower than 1.0 m. The maximum abrasion depth was at the shoreline, with values of 130 mm in 2004 and 278 mm in 2017. Based on the 27 years since seawall construction, front-side pillar abrasion was established as 10 mm/year. Abrasion depths on the sides and backs of the pillars were 160 and 100 mm, respectively, which were less than frontal values.

Figure 4 shows the planar distribution of bottom-plate abrasion depths for 2004 and 2017. The general tendency was similar to that of frontal surfaces, but abrasion depths were approximately triple.

Photo 1 Slit interiors

Photo 2 Abrasion

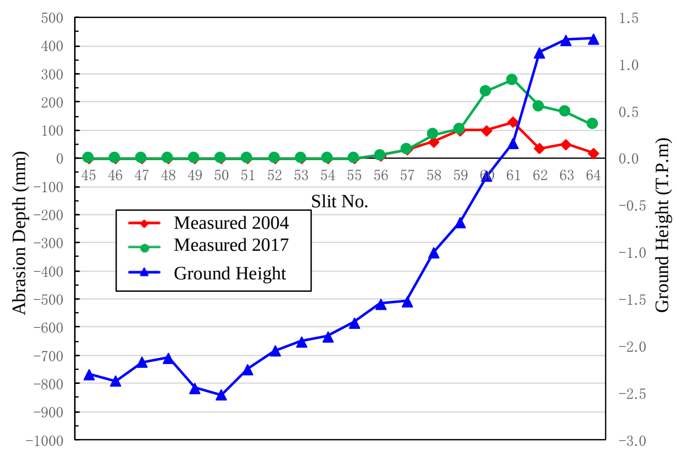

Fig. 3 Pillar-front abrasion depth

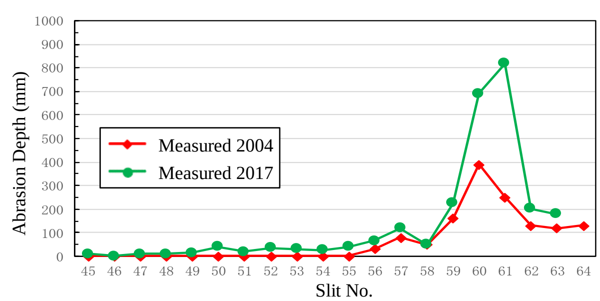

Fig. 4 Bottom-plate abrasion depth

EXPERIMENT

Experimental channel

In the study, a sea-bottom landform with a grade of 1:15 (24.0 m long, 0.6 m wide and 1.0 m deep) was created in a two-dimensional wave-making channel. A hydraulic characteristic experiment to determine water particle velocity/wave overtopping rate and a stone stabilization experiment were conducted with scales of 1/40 for the former and 1/20 for the latter in consideration of stone motion, and the on-site seawall shown in Fig. 1 was reproduced on these scales. All waves in the experiments were irregular, with 150 in each group. All values presented below are on-site.

1/20-scale experiment

The water depth d from the top of the stones to the still-water surface was taken as -0.5, 0.0, 0.5 and 1.0 m (Fig. 5). The wave period T_0' and the equivalent deep-water wave height H_0' were set as 7, 9, 11 and 13 s, and 0.50, 0.75, 1, 1.25, 1.50, 2, 2.50, 3 and 4 m, respectively. The stone mass was uniform at 100 kg. Those with the same mass were colored yellow, red and white from the front of the seawall and placed as shown in Photo 3, and stone movement was recorded using a digital video camera at the top of the seawall. Also, the stone layers was reproduced at 1.5 m thick as in the field. The resulting images were analyzed and temporal stone movement was determined to establish the collision rate. Water particle velocity upon collision was also monitored with a propeller current meter.

1/40-scale experiment

The wave period T_0' was uniform at 11.0 s, and the equivalent deep-water wave heights were 1, 2, 3, 4, 5, 6, 7 and 8 m. As shown in Fig. 6, a propeller current meter was positioned 4 m from the front of the seawall to monitor water particle velocity.
Wave overtopping was monitored via wave sluices for the patterns shown in Fig. 15, and the overtopping rates per unit width/time were determined from temporal volume/sluice width calculation. Nine wave heights were considered with a design condition of H_0' = 9.0 m.

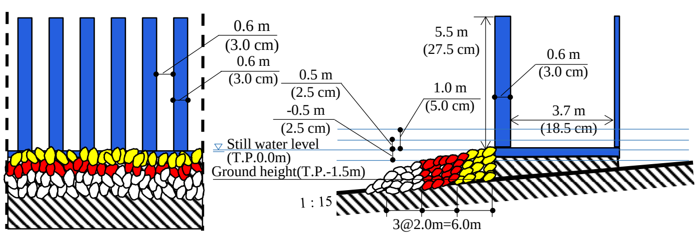

Fig. 5 Experiment section (scale: 1/20)

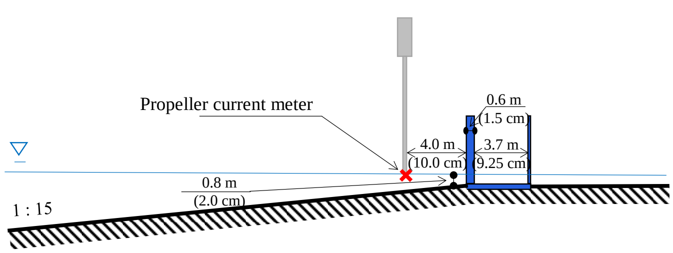

Fig. 6 Experiment section (scale: 1/40)

SEAWALL STONE MOVEMENT CHARACTERISTICS

Stone movement patterns

Photo 4 shows stone movement for d = 0.0 m, T_0' = 11.0 s and H_0' = 3.0 m. The high movement of white stones inside the slit suggests an increased likelihood of movement of those at the toe of the slope.
Collision frequency was calculated by totaling the number of stones remaining inside and the number of collisions determined from visual observation, and dividing the value by the number of slits (10) in the channel width. This frequency was then divided by 150 to determine the collision rate N (i.e., collision frequency per wave per slit).

Wave height and stone collision rate

Figure 7 shows the relationship between the stone collision rate N and the equivalent deep-water wave height H_0' for each water depth with T_0' = 11.0 s. The value obtained by interpolation exceeded N=0.01 for H_0' = 0.85 m at a depth of d = 0.0 m, for H_0' =1.40 m at a depth of 0.5 m and for H_0' = 1.70 m in other cases, roughly corresponding to the values calculated by Tanimoto et al.(1982). Shimazaki et al.(2018) also

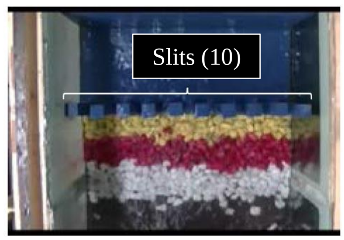

Photo 3 Before stone movement

Photo 4 After stone movement

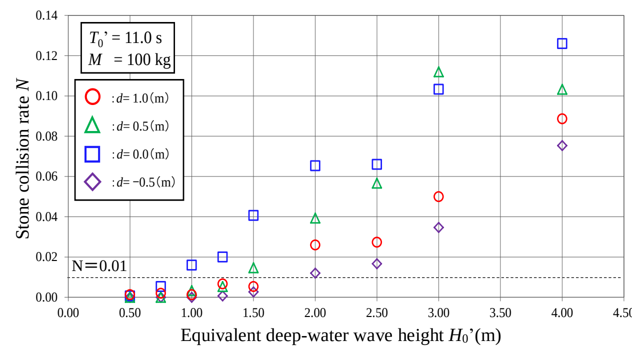

Fig. 7 Influence of water depth on collision rate

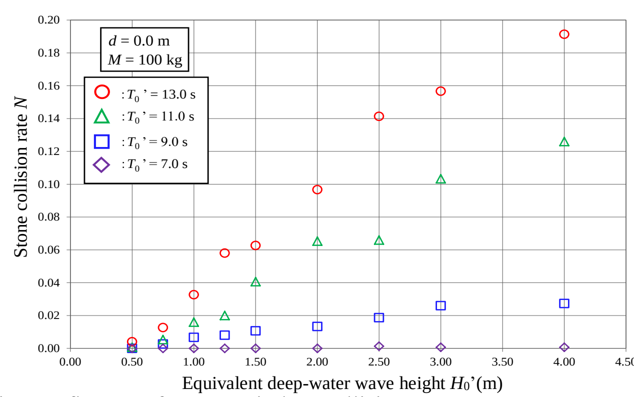

Fig. 8 Influence of wave period on collision rate

researched collision limits with stone masses under d = 0.0 m for consideration of related mass differences. For all water depth conditions, N increased dramatically for H_0' = 2.00 m or higher. Significant stone movement was observed with a water depth of d = 0.0 m, at which abrasion progressed at the actual site.

Figure 8 shows the relationship between the stone collision rate N and the equivalent deep-water wave height H_0' for each wave period at a depth of d = 0.0 m, where the most significant stone movement was observed. For T_0' = 7.0 s, no stone movement was observed. An increased collision rate was also observed for longer wave periods.

FLOW CHARACTERISTICS AT SLIT FRONTS

Relationship between water particle velocity and wave height

Figures 9 to 11 show the relationship between water particle velocity u_w and equivalent deep-water wave height H_0' for each wave period with the maximum flow rate u_{wmax}, the 1/20 maximum flow rate $u_{w1/20}$ and the 1/10 maximum flow rate $u_{w1/10}$. In consideration of variations in stone collision frequency per wave group with wave height conditions, the corresponding flow rates were determined from the data obtained. As the rate increase tended to stop around H_0' = 5.0 m in all wave periods, the stone collision rate detailed in stone movement characteristics was also considered to peak and stop increasing at H_0' = 5.0 m.

Stone collision frequency and velocity

The water particle velocity u_w at the time of stone collision was determined, and the relationship with collision velocity u_s is shown in Fig. 12. The average tendency for each wave period and height indicates collision velocity approximately 60% of water particle velocity. It was confirmed that these tendencies are similar under other periodic conditions.

Stone collision frequency is shown in Fig. 8 for certain wave periods and heights. Water particle velocity corresponding to collision frequency can be determined from the relationship between wave height and flow rate for each wave period (Figs. 9 to 11). Multiplying this value by 0.6 gives the stone collision velocity.

ESTIMATION OF CONCRETE ABRASION VOLUME

Abrasion volume calculation formula

The concrete abrasion volume (AD_M) was determined using the equation derived by Toyofuku et al. (1998) from indoor experiments.

$$AD_M = 10^{-2.2347} \cdot N^{0.5504} \cdot M_L^{0.4709} \cdot u_s^{1.2030} \cdot f_c^{-0.5074} \quad \cdots\cdots\cdots\cdots\cdots\cdots (1)$$

Here, N is the number of collisions, M_L is the stone mass, u_s is the collision velocity and f_c is concrete compressive strength. In abrasion volume estimation, the stone mass was uniform at 100 kg and the average concrete strength was 40 N/mm^2. Collision frequency and velocity over a period of two hours were also determined from the experiment results reported in stone movement and flow characteristics at slit fronts using two-hour significant wave height and wave period values from the nearest NOWPHAS station. This information was substituted into Eq. (1) to calculate the two-hourly abrasion volume.

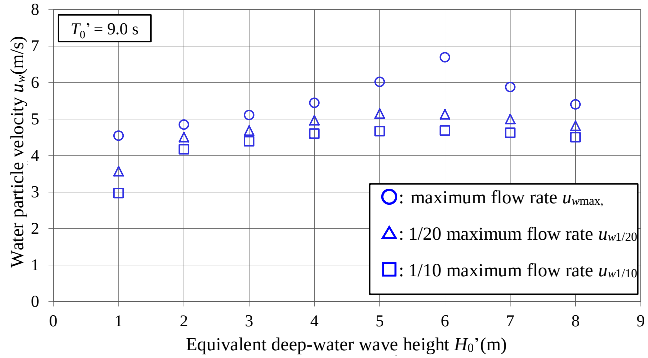

Fig. 9 Relationship between equivalent deep-water wave height and water particle velocity (T_0 '= 9 s)

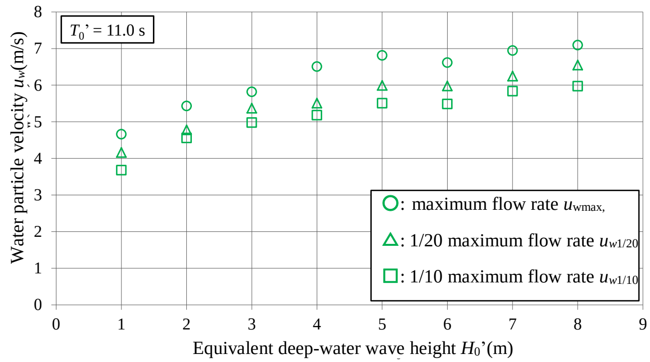

Fig. 10 Relationship between equivalent deep-water wave height and water particle velocity (T_0 '= 11 s)

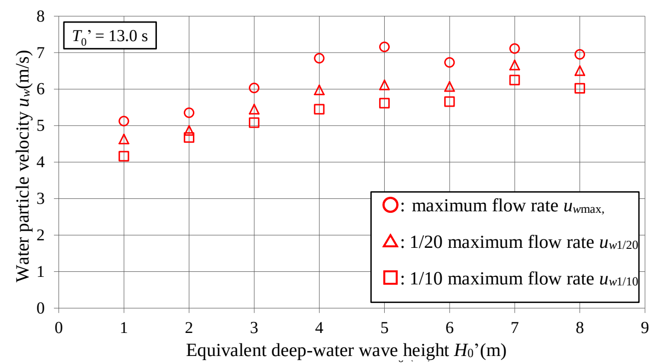

Fig. 11 Relationship between equivalent deep-water wave height and water particle velocity (T_0 '= 13 s)

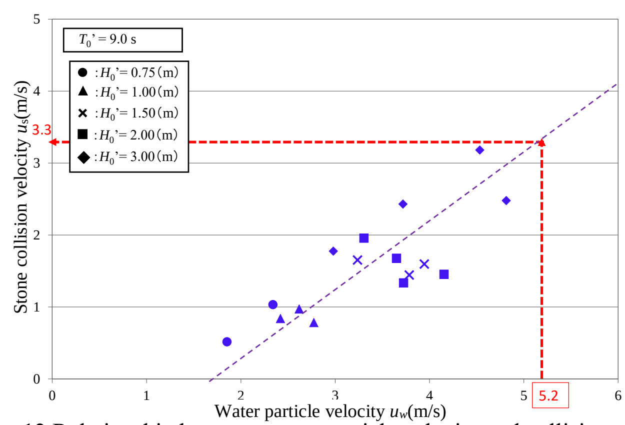

Fig. 12 Relationship between water particle velocity and collision velocity

Estimation of abrasion volume for conversion to model time

Figure 13 shows wave data obtained between March 31 and April 3, 2004, with a significant wave height of 4.4 m at 2 a.m. on April 2. Applying the experiment results presented in experiment gives an estimated collision frequency during 2 and 4 a.m. on that day of approximately 30 times this value.

As the significant wave period was 9.1 s, stone collision velocity can be estimated as approximately 2.8 m/s based on the experiment results reported in stone movement characteristics Substituting these values into Eq. (1) gives a two-hour abrasion volume of 0.17 mm. By performing this calculation for the two days when H_0' = 0.75 m or higher, the abrasion volume for conversion to the model time was found to be approximately 1 mm.

Temporal changes in abrasion volume

The same calculation as that for conversion to the model time was performed to total the abrasion volume for the service period and determine the overall value. Figure 14 shows the total abrasion volume by calendar year. The compressive strength of concrete was taken as –25, 40 and 55 N/mm^2. It can be seen that the total volumes in the 14th and 27th years (circled in the figure) roughly corresponded to the estimated total abrasion volume at 40 N/mm^2

REPAIR METHOD ANALYSIS

Cross-sectional shape

As splash-up of overtopping waves occurs at the site under normal wave conditions (Photo 5), it is necessary to maintain the wave-dissipating function of the slits. To determine an optimal repair method, the cross-sectional shapes shown in Fig. 15 were compared: (1) the existing slit-type seawall, (2) one with a worn part filled with concrete up to a height of 2.1 m, (3) one with wave-dissipating blocks at the front, and (4) one with slits completely filled with concrete (upright seawall). Wave overtopping experiments were conducted for each one.

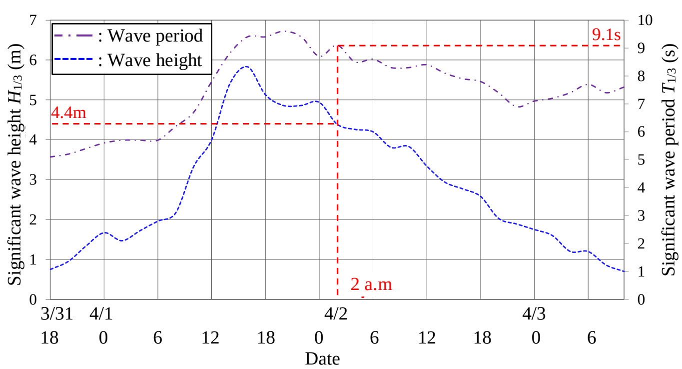

Fig. 13 Temporal changes in wave height and period

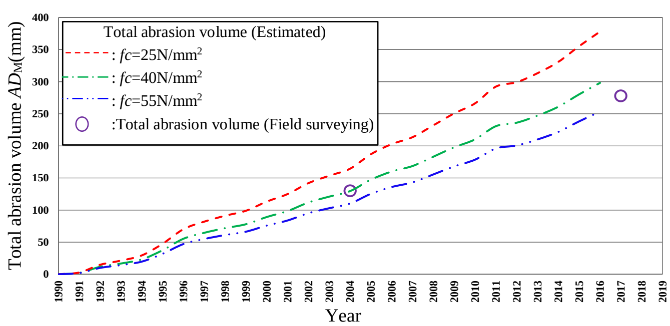

Fig. 14 Relationship between years and total abrasion volume

Optimal plan based on the overtopping wave flow rate

Figure 16 shows the relationship between the overtopping flow rate q and the equivalent deep-water wave height H_0' for each pattern. The rate

Photo 5 On-site wave overtopping

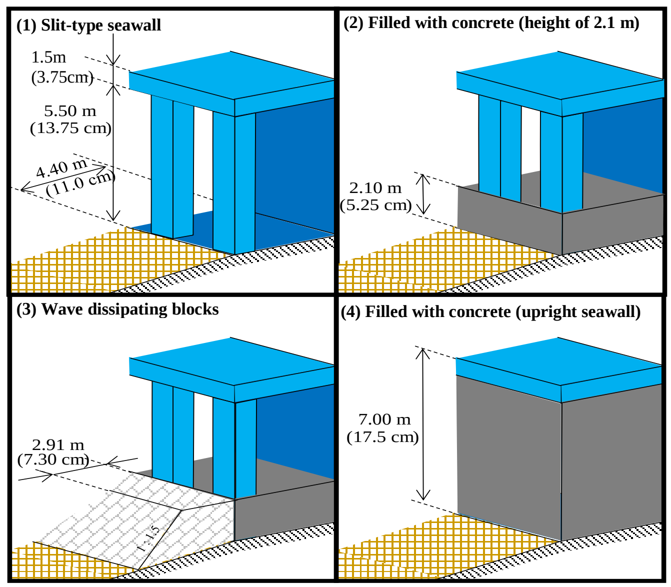

Fig. 15 Cross-sectional shapes of different patterns

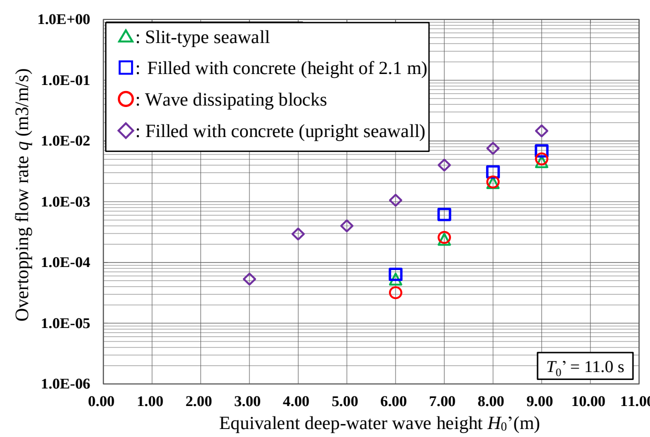

Fig. 16 Overtopping flow rate for each pattern

was the highest for the upright seawall, exceeding 1.0×10^{-2} m^3/m/s for a design wave height of H_0' = 9.0 m. For the other three, the rate was 1.0×10^{-4} m^3/m/s or lower when H_0' = 6.0 m, at which a local high-wave warning is issued, and vehicle safety was ensured. However, for H_0' =7.0 m or higher, the rate was higher for (2) than for (1) and (3).

The use of wave-dissipating blocks was considered optimal due to availability based on diverted materials at the site, in addition to the above experiment results. However, as abrasion of such blocks is also expected as with slits, regular field surveying and block replacement will be needed to prevent excessive wear and reduction of wave-dissipating performance.

CONCLUSIONS

The findings of the study can be summarized as follows:

(1) Seawall slit abrasion was deepest around T.P. 0.0 m, and was 278 mm at the maximum. The annual abrasion rate over 27 years was around 10 mm.

(2) The stone collision rate was the highest at a front water depth of 0.0 m, and corresponded to the on-site abrasion status. The collision rate also increased with longer wave periods.

(3) The relationship between equivalent deep-water wave height and stone collision velocity was determined from 1/20-scale model experiments to clarify stone movement. Study results also indicated that the slit flow rate stopped increasing at a deep-water wave height of 5 m.

(4) On-site abrasion volume was estimated by determining stone collision frequency and velocity using local wave observation data and the formula proposed by Toyofuku et al.

(5) Concrete filling for worn parts and placement of wave-dissipating blocks at the front was determined as the optimal method for slit-type seawalls.

This paper elucidates the abrasion characteristics of an actual slit-type seawall and presents a method for repair. Future work will involve research on the influence of different stone diameters on the abrasion rate, the effects of abrasion-resistant materials, and protection work to reduce impact.

ACKNOWLEDGMENTS

The authors are grateful to Koji Takahashi of Koken Engineering for his assistance in collecting on-site abrasion data, and to Professor Yasuji Yamamoto of Hokkaido University of Science for his contribution to the compilation of this paper.

REFERENCES

Matsuda K and Tsuno Y (2007). “Overall repair of the salt-damaged superstructure of the Tedorigawa River Bridge on the Hokuriku Expressway”, *Concrete Engineering*, Vol. 45, No. 11, pp. 821-825.

Oide Y and Takigahira M (2018). “Repair of eroded coastal retaining walls”, *FY 2017 Hokkaido Regional Development Bureau Research Presentation*, *Management-11 (road section)*.

Shimazaki K, Kimura K and Nagoshi T (2018), “Stone movement characteristics associated with wave action at the front of a slit-type seawall”, *73rd Annual Conference of the Japan Society of Civil Engineers*, II-206.

Tanimoto K, Yagyu T, Muranaga T, Shibata K and Goda Y (1982), “Stability of armor units for foundation mounds of composite breakwaters as determined via irregular wave tests”, *Report of the Port and Harbor Research Institute*, Vol. 21, No. 3, pp. 3-42.

Toyofuku T, Miyakawa K and Toyofuku T (1998), “A study on the characteristics of concrete impact abrasion”, *Proceedings of the Japan Concrete Institute*, Vol. 20, No. 2.

Watanabe K, Suwa Y, Sekiguchi Y, Noguchi K, Ito Y, Takada Y, Iwasa T and Nikaido R (2013). “Development of an accelerated test method for evaluating resistance to abrasion stress on gravel coasts”, *Journal of the Japan Society of Civil Engineers B3 (ocean development)*, Vol. 69, No. 2, I_832-I_837.